Energy Conversion and Management: X 17 (2023) 100341

Contents lists available at ScienceDirect

Energy Conversion and Management: X

journal homepage: www.sciencedirect.com/journal/energy-conversion-and-management-x

Analysis of partial heating supercritical CO_2 cycles bottoming small-power gas turbine units

Antonio Giuffrida *, Elham Akramieh

Politecnico di Milano, Dipartimento di Energia, Via R. Lambruschini 4, Milano 20156, Italy

ARTICLE INFO

Keywords:
Gas turbine
Partial heating cycle
Supercritical CO_2
Waste heat recovery

ABSTRACT

Supercritical CO_2 power systems are investigated as bottoming cycles of combustion turbines, limiting the power output of the topping cycle to the range of 5–10 MW. Actually, the conventional combined cycle with a bottoming steam power plant is not convenient for a number of commercial combustion turbines. In particular, the partial heating supercritical CO_2 cycle, with a limited number of components compared to other cycles, is the layout chosen in this work based on a relevant trade-off between heat recovery and cycle efficiency. Single-stage radial turbomachines are selected for the power system components, considering the investigated range of power production. Focusing on a number of cases, all related to commercially available combustion turbines, interesting considerations about the size of both turbomachinery and heat transfer equipment composing the supercritical CO_2 power cycle are possible thanks to scaling effects. However, proposing a customized supercritical CO_2 cycle for each combustion turbine is anything but a reasonably sound solution. Thus, a properly unified one-size-fits-all supercritical CO_2-based power system should be duly considered from a more practical point of view.

Introduction

Combustion turbines are a widely used technology in electric power generation as well as for aviation and marine ship power due to their high efficiency, compactness and flexibility. However, combustion turbine exhaust has large waste heat available. Actually, combustion turbines with power output of around 10 MW run with efficiency in the range of 30–35 % [1], so there is a lot of energy as waste heat in the exhaust gas. As a matter of fact, around 20 MW of thermal power can be recovered from a 10 MW combustion turbine, so small combustion turbines offer a serious opportunity for waste heat recovery. In detail, since utility and quality of the waste heat are determined by its available temperature, combustion turbines are in the middle quality range [2], though the exhaust temperature also depends on the operating load and environmental conditions.

Combining a bottoming cycle to a combustion turbine is an effective solution for exploiting the residual heat from the turbine exhaust. Additional energy can be produced and the final efficiency of the combined power system will increase. In general, recovering waste heat from thermal engines as well as industrial processes is one of the main pathways for cutting fossil fuel consumptions and carbon dioxide emissions, hence alleviating current severe energy and environmental situation.

Combined cycle thermal power plants have great interest in the field of power generation, due to their higher efficiency and lower environmental impact compared to combustion turbine cycles and steam Rankine cycle-based power plants independently. On the other hand, supercritical carbon dioxide (sCO_2) Brayton cycles have been investigated in the recent years as alternative bottoming cycles of combustion turbine units [3–7]. Initially proposed by Feher [8] and Angelino [9] around fifty years ago, compared to other power systems, sCO_2 cycles are simpler, offer a greater power density and have interesting cost advantage for the use of very compact equipment, which is a consequence of the high density and pressure of the working fluid [10].

The partial heating supercritical CO_2 cycle

There are lots of possible sCO_2 cycle layouts for power generation, even suitable for waste heat recovery applications [11]. They consist of many heat exchangers, compressors and turbines. However, an important feature for such cycles is the relatively simple layout. Fig. 1 shows the partial heating cycle, where two sCO_2 streams are separated at the outlet of the compression system (C): the first extracts heat in a low-temperature heater (LTH) and the second recovers heat in a recuperator (REC), then the two streams meet before entering a high-

* Corresponding author.
E-mail address: antonio.giuffrida@polimi.it (A. Giuffrida).

https://doi.org/10.1016/j.ecmx.2022.100341
Received 5 October 2022; Received in revised form 23 November 2022; Accepted 4 December 2022
Available online 5 December 2022

Nomenclature

a	speed of sound, $m \cdot s^{-1}$
A	area, m^2
AMC	Acceleration Margin to Condensation
CR	heat capacity rate ratio
D	diameter, m
h	specific enthalpy, $J \cdot kg^{-1}$
HT	high temperature
HTH	high temperature heater
LMTD	log mean temperature difference, K
LT	low temperature
LTH	low temperature heater
$\dot{m}$	mass flow rate, $kg \cdot s^{-1}$
Ma	Mach number
Ns	specific speed
NTU	number of transfer units
Q	volumetric flow rate, $m^3 \cdot s^{-1}$
$\dot{Q}$	heat transfer rate, W
R^2	coefficient of determination
REC	recuperator
sCO_2	supercritical carbon dioxide
SR	speed ratio
T	temperature, K
u	peripheral velocity, $m \cdot s^{-1}$
U	overall heat transfer coefficient, $W \cdot m^{-2} \cdot K^{-1}$
UA	product of overall heat transfer coefficient and heat transfer area, $W \cdot K^{-1}$

Greek letters

Δ	difference
φ	flow coefficient
ω	rotational speed, $rad \cdot s^{-1}$

Subscripts

C	Compressor
in	inlet station
is	isentropic
out	outlet station
T	turbine

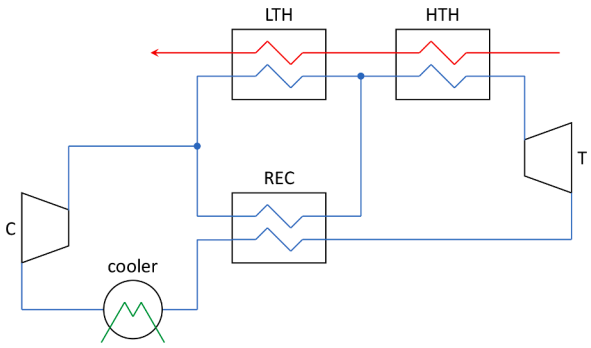

Fig. 1. Schematic layout of the partial heating sCO_2 cycle for waste heat recovery (stream in red). (For interpretation of the references to colour in this figure legend, the reader is referred to the web version of this article.)

temperature heater (HTH) and expanding through the turbine (T). The stream exiting the turbine passes through a recuperator to transfer heat to the low-temperature fluid, then through a cooler before entering the compressor (C). This power cycle has been studied in a number of works dealing with waste heat recovery [4–6,12–14], although higher efficiency could be achieved by more complex cycles. In particular, Li et al. [14] evaluated and compared six sCO_2 cycles for waste heat recovery of combustion turbine, but they finally recommended the partial heating sCO_2 cycle as the most potential cycle according to its low economic cost, simple system architecture and high total heat recovery efficiency. After realizing the advantages of this sCO_2 cycle for harvesting the exhaust gas waste heat, a number of researchers have recently oriented their investigations also to the optimal heat exchanger allocation [15], the part-load operation strategies and off-design performance [16,17] as well as the integration of the partial heating sCO_2 cycle in more complex system layouts [18–20].

Recent investigations by Bonalumi et al. [21,22] have focused on sCO_2 cycles bottoming a 4.7 MW combustion turbine. After setting a proper limit for the turbomachinery load, around 1600 kW can be recovered by the partial heating cycle, though a techno-economic optimization would guide towards an optimum point with slightly more than 1500 kW of power output and a specific cost for the technology of around 2000 $/kW [21]. Later, investigations of the single-heated cascade cycle [22] in place of the partial heating cycle have highlighted no significant improvement for the power output. This result has been achieved despite a slightly more complicated cycle layout with two expanders and a compressor whose shaft rotates more slowly compared to the turbines. In detail, the two turbines can certainly rotate on the same shaft, but directly driving the compressor at the turbine rotational speed is not possible, as emerged from preliminary considerations about (i) the size of the turbomachinery impellers and (ii) the passage areas for flow rate accommodation [22]. As a matter of fact, the impossibility of direct matching compressor and turbine shafts had never been previously addressed in other literature works dealing with cascade cycle architectures [3,5,6,11,13], mostly focused on cycle thermodynamics. Further calculations of more complex cycle architectures, even including intercooled compression, compared to both the partial heating and the single-heated cascade cycles have been carried out as well. Anyway, the performance improvements are not much more interesting in comparison to the partial heating cycle, especially if attention is paid also to technical issues of the sCO_2-based power system components.

Aim and novelty of the work

According to the considerations above and to thorough investigations of the partial heating sCO_2 cycle as reported in a previous study [21], the current work focuses again on the partial heating sCO_2 cycle, as an interesting cycle architecture with simple layout and a limited number of components. In detail, this work aims at extending the analysis of the partial heating sCO_2 cycle in combined cycles where combustion turbines with power output in the range of 5–10 MW are used as topping cycle. Actually, these combustion turbines combined with a sCO_2-based power system would maintain the advantage of compactness and increase the overall efficiency of the power plant.

Starting from those solutions and conclusions and adopting the same approach [21], attention is here paid (i) to the thermodynamics of the sCO_2 cycle and (ii) to its components as regards the compressor, the turbine and the heat exchangers. Interesting considerations about the size of these components, along with scaling effects, are reported as well as specific remarks about the possibility to use the proposed research. As a matter of fact, the proper design of a unified one-size-fits-all sCO_2-based power system should be considered as a good solution from a more practical point of view.

Table 1
Specifications and performance of combustion turbines as input data for the calculations [1].

No.	Power, MW	Efficiency, %	Gas flow rate, kg/s	TOT, °C
1	4.71	32.6	17.4	511.0
2	5.05	30.2	19.5	545.0
3	5.38	32.3	21.3	493.9
4	5.40	31.0	20.9	541.0
5	5.47	29.5	21.7	541.7
6	5.53	29.6	21.7	545.0
7	5.67	31.5	21.6	510.0
8	5.82	32.2	21.4	522.2
9	6.50	33.1	21.2	537.8
10	6.63	32.2	26.1	505.0
11	6.74	30.3	27.0	512.8
12	6.80	30.3	27.0	515.6
13	7.80	33.6	27.2	522.8
14	7.80	33.2	29.4	490.0
15	7.90	30.6	30.2	542.2
16	8.18	34.4	26.7	515.6
17	8.60	34.2	30.3	504.4
18	10.36	34.8	33.8	507.8

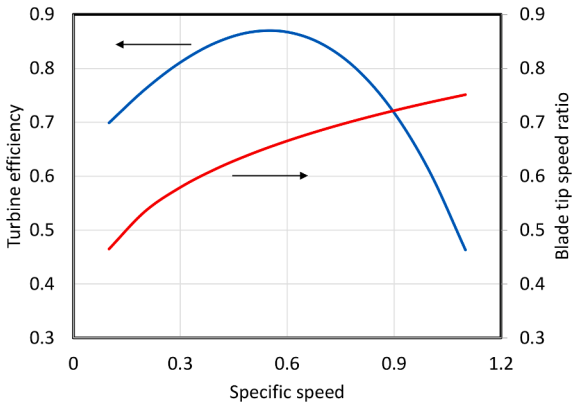

Fig. 2. Isentropic efficiency and speed ratio of the radial-inflow turbine [32].

Calculation of the sCO_2 cycles

This section includes some brief considerations about the calculation assumptions for the sCO_2 cycle, though more detailed information is reported in a previous work [21]. In particular, attention is paid to (i) the sCO_2 temperature at compressor inlet, (ii) the selection of compressor and turbine efficiency values, (iii) the load set for the compressor and (iv) the calculations of the heat exchangers because of the significant variation of CO_2 specific heat capacity under different temperatures and pressures.

Initially, a list of combustion turbines with power output in the range of 5–10 MW, as the scope in this work, is reported in Table 1. The combustion turbine market offers a number of units for this power range and Table 1 details various performance figures. Specifications of efficiency, exhaust gas flow rate as well as turbine outlet temperature (TOT) [1] are included, without reporting any information related to manufacturers and models just to avoid commercialism.

As regards the sCO_2 cycle calculations, it is worth highlighting that lots of researchers set compressor inlet conditions relatively near to the two-phase region, with a minimum cycle temperature as low as 32 °C [3,4,13,14,23–28]. Actually, low CO_2 temperatures at compressor inlet reflect on lighter compression works. This result is due to the higher CO_2 density near to the critical point, where the temperature is around 31 °C. Nevertheless, possible phase change in the inlet flow passages of the compressor is not duly taken into account and such an event could occur owing to local flow acceleration causing reduction in static pressure and temperature. A non-dimensional criterion named Acceleration Margin to Condensation (AMC) was introduced by Monje et al. [29,30], who proposed and quantified the margin between the expected fluid properties in the inducer and the saturation line. In detail, they defined the AMC as the Mach number at the throat of the impeller when the static properties of the fluid lie on the saturation line and suggested a reference value of AMC equal to 0.6 [29,30]. Based on this figure, the minimum sCO_2 cycle temperature in this work is set at 40 °C. On the other hand, lower temperatures will require water as cooling carrier for heat rejection, which should be as cold as possible, thus limiting the applicability only to some specific geographical areas.

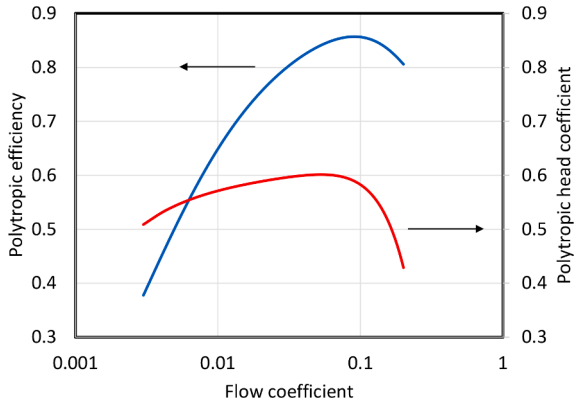

Fig. 3. Polytropic efficiency and head coefficient of the centrifugal compressor [33].

Turbomachinery performance strongly affects the overall cycle efficiency [31]. In detail, a radial-inflow turbine and a centrifugal compressor, both as single-stage turbomachinery, are considered in this work. As regards the turbine, the approach suggested by Aungier [32] is adopted. Fig. 2 shows the isentropic efficiency depending on the specific speed of the turbine:

$$Ns_T = \omega_T \bullet \frac{\sqrt{Q_{out_{is,T}}}}{\Delta h_{is,T}^{0.75}} \quad (1)$$

When Ns_T is equal to 0.55, it is possible to achieve the maximum efficiency, i.e. 0.87 [32]. In detail, the rotational speed of the turbine shaft results from Eq. (1). As a matter of fact, the enthalpy drop can be quickly determined after setting the maximum sCO_2 cycle temperature as well as inlet and outlet turbine pressures and the CO_2 flow rate results from an energy balance at the high-temperature heat exchanger (HTH in Fig. 1). Fig. 2 also details the speed ratio:

$$SR = \frac{u_T}{\sqrt{2 \bullet \Delta h_{is,T}}} \quad (2)$$

Thus, the blade peripheral velocity (u_T) and the rotor diameter are calculated based on the enthalpy drop and the speed ratio [32].

As regards the compressor, the rotational speed is the one previously calculated for the turbine. Fig. 3 summarizes the approach proposed by Aungier for centrifugal compressor performance assessment [33], suggesting optimal values of polytropic efficiency and head coefficient as functions of the flow coefficient:

$$\varphi_C = \frac{4 \bullet Q_{in,C}}{\pi \bullet D_C^2 \bullet u_C} \quad (3)$$

According to Aungier's approach, the diameter of the compressor impeller can be finally calculated.

Always referring to the compressor, it has been anticipated that the minimum cycle temperature and the AMC value have been set equal to 40 °C and 0.6, respectively. A former work [21] thoroughly investigated both the minimum and maximum cycle pressures in order to achieve the best sCO_2 cycle performance. Actually, cycle pressure variations affect the compressor load, which can be related to the compressor Mach

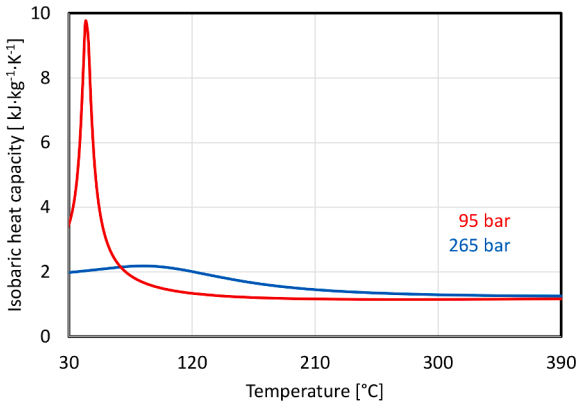

Fig. 4. Isobaric heat capacity for CO_2 as a function of temperature at two pressure levels.

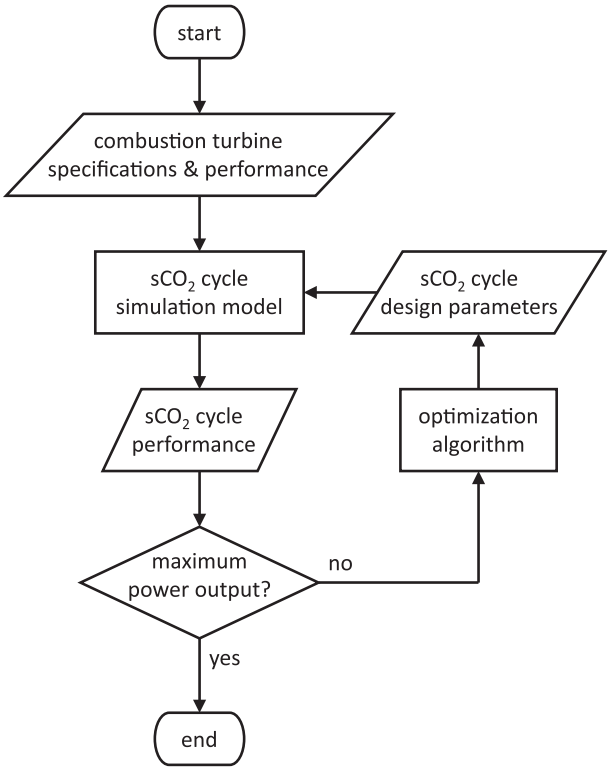

Fig. 5. Schematic solving procedure for assessing the performance of the sCO_2 cycle.

number (Ma_C). The latter is the ratio between the impeller peripheral velocity and the speed of sound of the working fluid at the turbomachinery inlet:

$$Ma_C = \frac{u_C}{a_{in,C}} \tag{4}$$

Based on previous parametric analyses [21], the minimum cycle pressure and the compressor Mach number are set equal to 95.6 bar and 0.85, respectively, for the new cycle calculations. As for the CO_2 pressure at the compressor outlet, calculations show that it is around 265 bar, with really negligible variations from case to case.

Focusing on the heat exchangers in the sCO_2 cycle layout, a specific feature is the UA product:

$$UA = \frac{\dot{Q}}{LMTD} \tag{5}$$

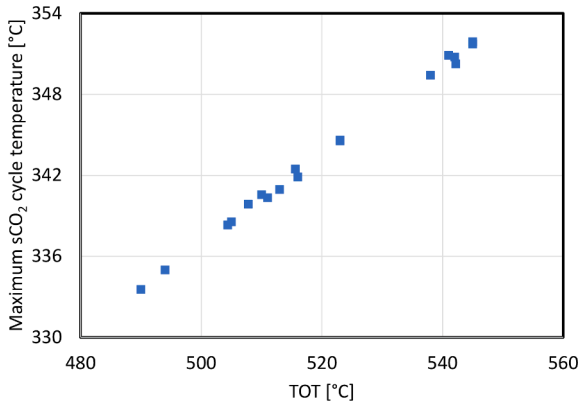

Fig. 6. Maximum sCO_2 cycle temperature vs gas temperature at combustion turbine outlet (TOT).

In detail, U is the overall heat transfer coefficient, A is the heat transfer area, $\dot{Q}$ is the heat transfer rate and LMTD is the log mean temperature difference across the heat exchanger. However, considering CO_2 specific heat capacity significantly varies under different temperatures and pressures, as detailed in Fig. 4, the non-linear trends of the thermal profiles must be duly taken into account [34]. Thus, a proper value of the UA product for each heat exchanger present in the layout schematized in Fig. 1 is calculated and reported in the next section. In detail, each heat exchanger is divided into one hundred segments and the overall LMTD results as

$$LMTD = \left(\frac{1}{\dot{Q}} \bullet \sum_j \frac{\dot{Q}_j}{LMTD_j} \right)^{-1} \tag{6}$$

Other main calculation assumptions are the temperature difference at the cold side of the high-temperature heater (HTH in Fig. 1) and the effectiveness of the recuperator, which are set equal to 20 K and 0.9, respectively. As regards further assumption and calculation details, the reader is addressed to the previous work [21].

In addition, use of the REFPROP database [35] is made throughout the cycle calculations, according to the equation of state proposed by Span and Wagner [36].

Fig. 5 outlines the solving procedure adopted in this research by means of a basic flow chart. After inputing specifications and performance for each combustion turbine, according to the details in Table 1, as well as the main design parameters of the sCO_2 cycle, the calculation procedure is run until the maximum power output is obtained. An optimization solver controls this target by modulating two specific design parameters, namely the flow splitting fraction at the compressor outlet and the maximum cycle temperature (all the other cycle parameters are frozen as fixed assumptions). In particular, the latter is worth of attention, as reported in the next section.

Results

This section deals with the results obtained after running the sCO_2 power cycle simulations. In detail, as many cases as the combustion turbines whose specifications are included in Table 1 are reported and discussed.

Focusing on the sCO_2 cycle thermodynamics, a clear result is shown in Fig. 6, where higher exhaust gas temperatures reflect on higher maximum temperature of the sCO_2 cycle, i.e. the CO_2 temperature at the inlet of the radial turbine. Neither the combustion turbine efficiency nor the exhaust gas flow rate seem to affect the trend in Fig. 6. This result is certainly beneficial to the cycle efficiency, also considering that the minimum cycle temperature is always fixed as a calculation assumption (40 °C).

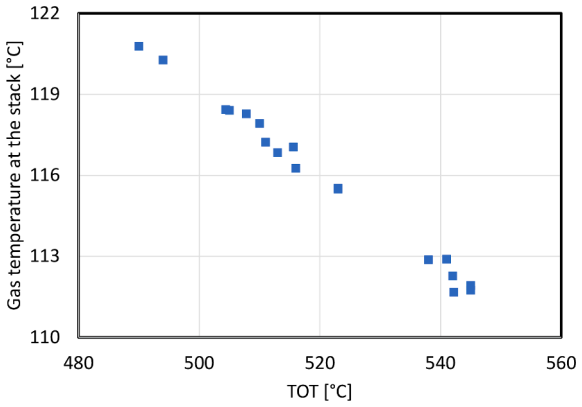

Fig. 7. Gas temperature at the stack vs gas temperature at combustion turbine outlet (TOT).

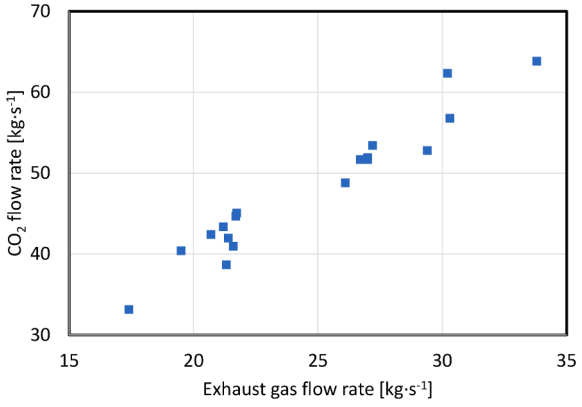

Fig. 8. CO_2 flow rate vs exhaust gas flow rate at combustion turbine outlet.

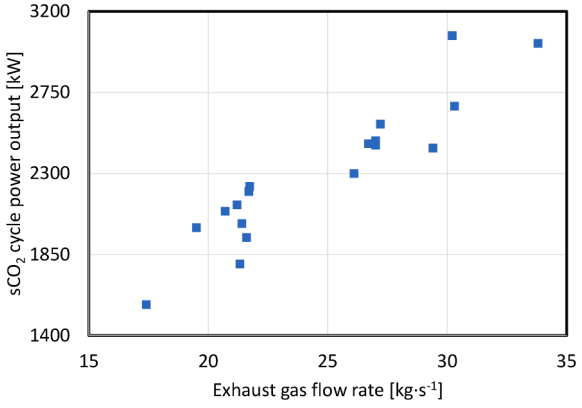

Fig. 9. Power production at the bottoming cycle vs exhaust gas flow rate at combustion turbine outlet.

In addition, when considering cases of combustion turbines with higher TOT, the exhaust gas at the cold side of the low-temperature heater is released less and less warmer. This result, as shown in Fig. 7, is interesting from the point of view of the heat recovery, though it does not seem to be immediately justifiable. Thus, attention is paid to the results of CO_2 mass flow rate throughout the bottoming closed cycle.

Actually, as detailed in Fig. 8, the higher the exhaust gas flow rate, the higher the CO_2 flow rate. These flow rates are an interesting figure suggesting the size of the bottoming power system components, as presented in the following. However, the trend in Fig. 8 is not so regular as the one in Fig. 6 and results from different values of efficiency of the

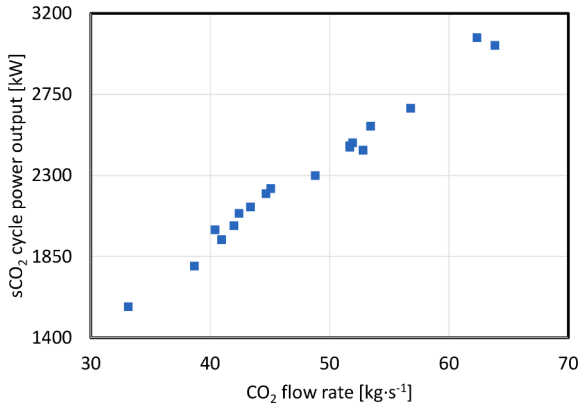

Fig. 10. Power production at the bottoming cycle vs CO_2 flow rate.

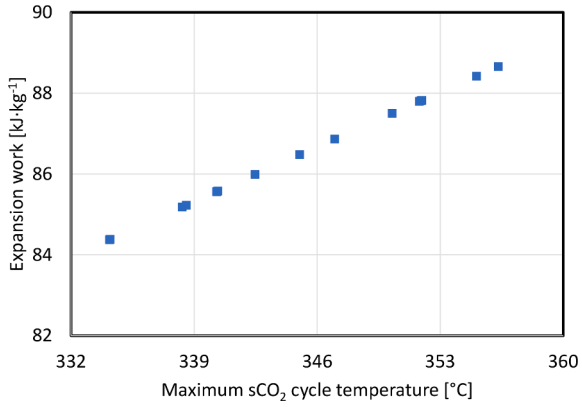

Fig. 11. Expansion work at the bottoming cycle vs maximum cycle temperature.

combustion turbine and, in particular, TOT (see Table 1). As an example, attention is paid to cases 15 and 17, with almost the same gas flow rate (30.2 and 30.3 kg/s) and two different TOT values (542.2 °C and 504.4 °C). As a matter of fact, the lower TOT directly reflects on the heat per unit mass that can be recovered to drive the sCO_2 cycle, so less CO_2 flows throughout the bottoming cycle for case 17 compared to case 15. Always focusing on these two cases and returning to Fig. 7, the gas exits the low-temperature heater at different temperatures (118.4 °C for case 17 and 111.7 °C for case 15). Thus, two values of CO_2 flow rate in Fig. 8 for almost the same gas flow rate are justified for these two cases, but similar considerations can be repeated for other singular cases in Fig. 8. Of course, singularities in CO_2 flow rate will also reflect on different heat duty of the high- and low-temperature heaters.

Fig. 9 reports the power output of the sCO_2 cycle as a function of the exhaust gas flow rate, but the same singularities already highlighted in Fig. 8 are evident in Fig. 9. Once again, attention is paid to cases 15 and 17, with almost the same exhaust gas flow rate, and the power production at the sCO_2 cycle is higher for case 15 (3066 vs 2674 kW). This result can be simply justified as the higher TOT reflects on higher CO_2 flow rate for case 15. On the other hand, when replacing the exhaust gas flow rate with the CO_2 flow rate according to Fig. 8, the new trend in Fig. 10 is more regular.

However, focusing on the power output of the sCO_2 cycle, there is another factor which plays a significant role together with the mass flow rate, i.e. the expansion work as shown in Fig. 11. Actually, the greater power output is the result not only of greater CO_2 flow rate but also of different values of the maximum sCO_2 cycle temperature (see Fig. 6). In detail, the compression work is almost constant (around 30 kJ/kg) for all the cases as the result of the fixed Mach number (0.85) for the compressor, but the expansion work increases with higher maximum

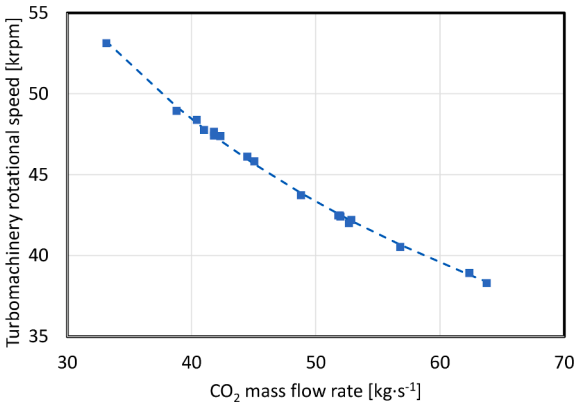

Fig. 12. Turbomachinery rotational speed vs CO_2 flow rate.

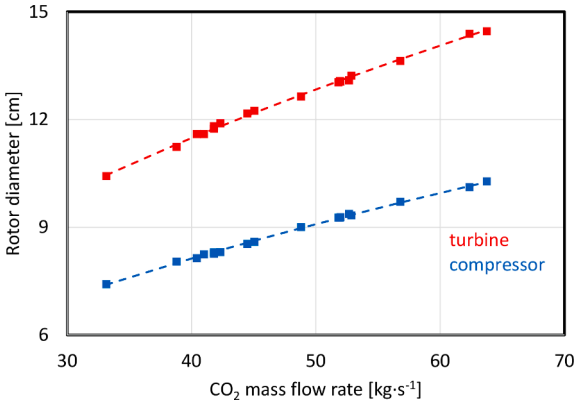

Fig. 13. Turbomachinery rotor diameters vs CO_2 flow rate.

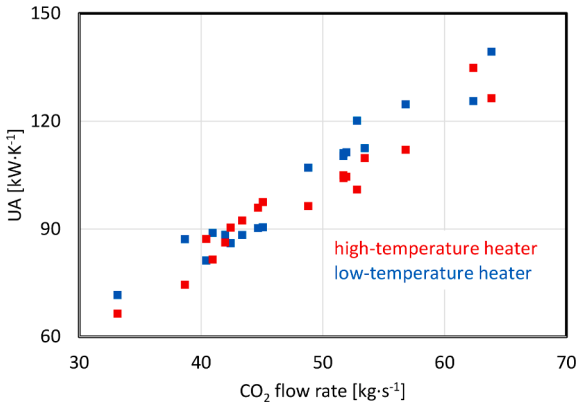

Fig. 14. UA values for both high- and low-temperature heaters.

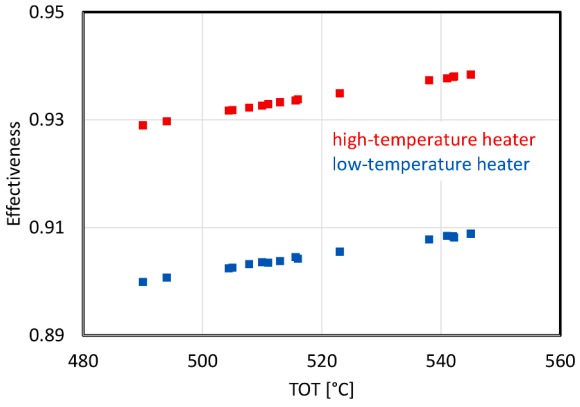

Fig. 15. Effectiveness values for both high- and low-temperature heaters.

cycle temperature. As a matter of fact, the minimum cycle pressure is fixed and the maximum cycle pressure (around 265 bar) results from the selected compressor Mach number. Thus, the higher the maximum sCO_2 cycle temperature, the higher the enthalpy drop across the turbine, as reported in Fig. 11.

If some of the considerations above can result from scaling effects, attention is now paid to the cycle components, with particular reference to compressor and turbine. As anticipated in the previous section, the specific speed of the turbine (Ns_T) is always fixed at 0.55 for the maximum isentropic efficiency (0.87). Thus, Eq. (1) can be interestingly revised to find a relation between the rotational speed and the mass flow rate. Based on the sCO_2 cycle thermodynamics, when the maximum temperature increases (see Fig. 6), the enthalpy drop across the turbine rises, as reported in Fig. 11, but a similar trend can be appreciated also for the specific volume at the end of the expansion process. Thus, it is possible to justify the results shown in Fig. 12 where the rotational speed is inversely proportional to the square root of the CO_2 mass flow rate (R^2 >0.99).

In compliance with this trend, Fig. 13 details greater rotor diameters for both compressor and turbine when the CO_2 flow rate increases. Similarly to Fig. 12, the dotted lines in Fig. 13 are used to highlight a specific trend: in this case, the rotor diameter is proportional to the square root of the CO_2 flow rate. Nevertheless, this result is not surprising because the turbomachinery load depends on the peripheral velocity of the impeller, which is almost constant for the compressor and slightly variable for the turbine (see Fig. 11). Thus, based on Eq. (1), the square root trends in Fig. 13 are fully justified and turbomachinery size correctly increases for accommodating larger flow rates.

Looking at Fig. 1, in addition to one compressor and one turbine, there are four components as heat transfer equipment. Attention is first paid to both the high- and low-temperature heaters (HTH and LTH in Fig. 1) and Fig. 14 reports the UA products, where U is the overall heat transfer coefficient and A is the heat transfer area. As shown in the figure, the higher the CO_2 flow rate, the greater the UA product. In detail, the mass flow rate reported in the horizontal axis refers to the stream passing through the high-temperature heater, before expanding through the turbine. As a matter of fact, the CO_2 flow rate through the low-temperature heater is lower due to flow splitting at the compressor outlet (see Fig. 1).

From a heat transfer point of view and focusing on the CO_2 path for the sake of simplicity, the heat transfer rate is

$$\dot{Q} = UA \bullet LMTD = \dot{m}_{CO2} \bullet \Delta h_{CO2} \quad (7)$$

Considering the ratio between enthalpy difference and LMTD does not experience significant variations for the investigated cases, a kind of proportionality between UA values and mass flow rates is justified. Thus, the higher the flow rate, the bigger the dimensions of the heat exchanger, so UA can be revised as a figure of the size of the heat transfer equipment.

In detail, the UA values reported in Fig. 14 for both the high- and low-temperature heaters are very close to each other. This result can be justified after considering that the heat transfer rate at the high-temperature heater is around 2.2–2.3 times greater than at the low-temperature heater. However, the latter is characterized by a much lower LMTD, as it is possible to realize according to the temperature values in (i) Table 1, (ii) Figs. 6 and 7 and (iii) the temperature difference at the cold side of the high-temperature heater which is set equal to 20 K throughout the calculations. As a further detail, focusing on case 1 as an example, the temperature profiles as functions of the heat transfer rate for these heat exchangers are reported in the Appendix A.

Another result for both high- and low-temperature heaters is shown

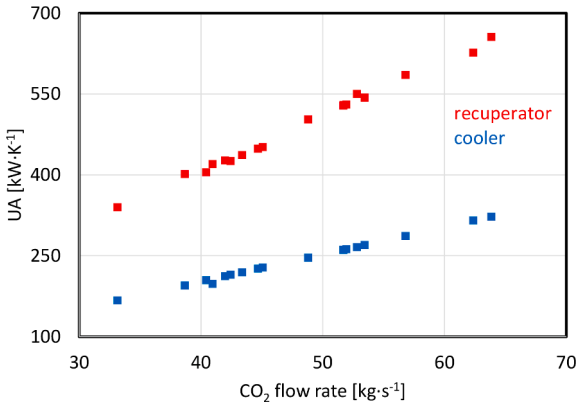

Fig. 16. UA values for recuperator and cooler.

in Fig. 15, where the effectiveness slightly increases in case of higher TOT. Actually, after setting a specific flow arrangement, the effectiveness of a heat exchanger depends on the number of transfer units (NTU) and on the heat capacity rate ratio (CR) [37]. In detail, the effectiveness increases for higher NTU and fixed CR as well as for lower CR and fixed NTU [37]. Focusing on the high-temperature heater, for the sake of brevity, calculation results suggest a weak increase of the number of transfer units (almost equal to 3.7) as well as a slight reduction of the heat capacity rate ratio (almost equal to 0.44) in case of higher TOT. Both these results are fully sufficient to justify the trends in Fig. 15, where effectiveness values always lower than 0.94–0.95 are reported, beyond which the cost of the heat transfer equipment would rise unsustainably [38].

Along with the high- and low-temperature heaters, Fig. 1 shows the sCO_2 cycle also requires a recuperator and a cooler. In detail, the recuperator is the heat exchanger with the highest UA value [21] and a rate of heat transfer around 1.2–1.3 times higher compared to the high-temperature heater. Fig. 16 shows the UA product at the recuperator as a function of the CO_2 flow rate at the turbine outlet, i.e. at the hot path of the heat exchanger (see Fig. 1). In this case, the reported trend is more regular in comparison with the ones in Fig. 14 where some scattering is evident. In particular, compared to the UA values in Fig. 14, differences are significant even though the technology of these heat exchangers is not the same: fin tube for the high- and low-temperature heaters vs printed circuit for the recuperator [39].

Always in Fig. 16, another regularly linear trend can be appreciated for the UA product at the cooler. As regards the heat rejection, the ratio between the heat duty at the cooler and the one at the high-temperature heater is around 1.1, slightly lower than the recuperator. However, lower UA values compared to the recuperator result in this case because of the higher LMTD at the cooler.

Final remarks

The results presented and discussed in the previous section specifically refer to calculations of bottoming sCO_2 cycles related to about twenty commercial combustion turbines with power output from 5 MW to 10 MW (see Table 1). These results can be enlarged in case of raising the power threshold up to 15 MW or even more. In detail, the combustion turbine market offers less than ten units with power output in the range of 10–15 MW so, based on the current results, it is not difficult to imagine the performance behaviour of other sCO_2 cycles as bottoming solutions for more powerful combustion turbines. However, when considering the recovery of larger amounts of waste heat, the radial turbine could be replaced by axial-flow turbomachinery, even multi-stage, due to better expansion efficiency [31]. Actually, the selection of an axial-flow instead of a radial-flow expander lies outside the scope of the current work, which is oriented to consider sCO_2 bottoming cycles as compact as possible for definitely improving the performance of small-power combustion turbines.

Nevertheless, an ultimate consideration is necessary. The results of specific calculations referring to a number of small combustion turbines are presented in this work. Even considering the market of these power generation systems, a customized sCO_2 cycle for each combustion turbine is anything but a reasonably sound proposal. Thus, a smart standardization should be suggested at least at the thermodynamic level, resulting in a unified bottoming cycle with the same turbine inlet temperature and pressure, as well as other thermodynamic parameters in common. On the other hand, different combustion turbines have different exhaust gas temperatures and mass flow rates, as already detailed in Table 1. These features could prevent the creation of unified cycle components otherwise particularly designed for each specific case. Thus, if time of development and final investment are very strict, then the proper design of a unified one-size-fits-all sCO_2-based power system should be considered as a good solution. Of course, the cost of standardization will reflect on efficiency and power output, since some of the waste heat in the exhaust gas will be inevitably lost.

Conclusions

According to the calculation methodology adopted in a former study and starting from those previous results [21], partial heating sCO_2 cycles as bottoming power systems of small combustion turbines have been investigated in this work. In detail, the current analysis has been oriented to sCO_2 cycle calculations referring to combustion turbines with power output from 5 MW to 10 MW.

Considering that about twenty cases of small combustion turbines have been investigated, with various features as detailed in Table 1, first conclusions are reported as regards the thermodynamics of the sCO_2 cycle: the higher the exhaust gas temperature, the higher the maximum sCO_2 cycle temperature, which leads to higher turbine work. At the same time, effectiveness values for both the high- and low-temperature heaters slightly increase according to higher TOT. On the other hand, when focusing on the exhaust gas flow rate, a clear relation can be found with the power output of the sCO_2 cycle, which really benefits from the use of single-stage radial turbomachinery. The higher the exhaust gas flow rate, the higher the power output of the sCO_2 cycle as well as the larger the turbomachinery dimensions. In detail, according to Aungier's correlations [32,33], which also allow for a preliminary turbomachinery sizing, the diameters of both compressor and turbine impellers increase according to the square root of the CO_2 flow rate. The higher the mass flow rate, the lower the rotational speed since it is inversely proportional to the square root of the CO_2 flow rate. Ultimately, the UA parameter of the heat exchangers, calculated as the product of the overall heat transfer coefficient and the heat transfer area, also increases with the CO_2 flow rate.

As a concluding remark, proposing a customized sCO_2 cycle for each combustion turbine does not seem to be a reasonable solution. Thus, a properly unified one-size-fits-all sCO_2-based power system should be duly considered from a more practical point of view. A thorough analysis of the combustion turbine market, along with considerations about the most best-selling unit in the investigated power range (5–10 MW), will guide further specific investigations as future developments of the current research.

CRediT authorship contribution statement

Antonio Giuffrida: Conceptualization, Methodology, Software, Validation, Data curation, Writing – original draft, Writing – review & editing, Visualization, Supervision. **Elham Akramieh:** Methodology, Software, Validation, Investigation, Data curation, Writing – review & editing.

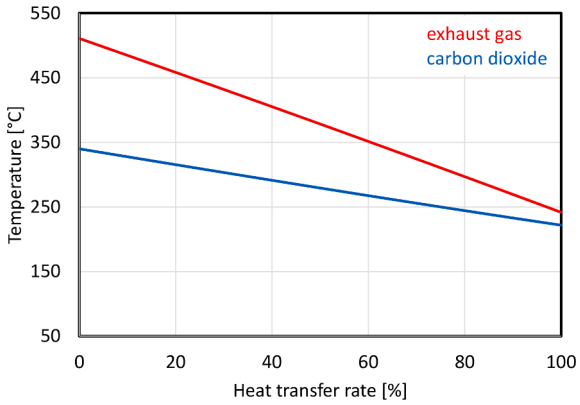

Fig. A1. Temperature profiles as functions of the heat transfer rate at the high-temperature heater for case 1.

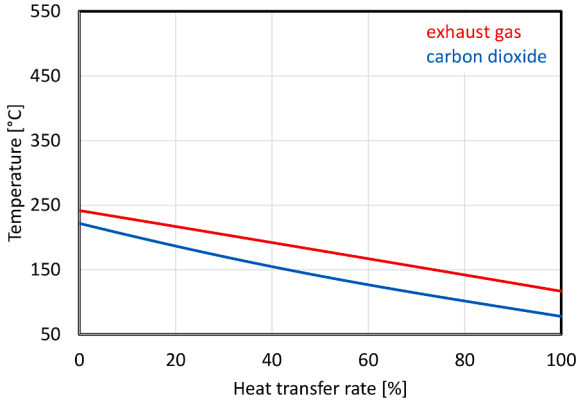

Fig. A2. Temperature profiles as functions of the heat transfer rate at the low-temperature heater for case 1.

Declaration of Competing Interest

The authors declare that they have no known competing financial interests or personal relationships that could have appeared to influence the work reported in this paper.

Data availability

Data will be made available on request.

Appendix A

This section reports two plots with the temperature profiles for the high-temperature heater (in Fig. A1) and the low-temperature heater (in Fig. A2), referring to case 1 in Table 1 as an example, but similar plots result from the analysis of the other cases. Looking at these two figures, it is possible to realize that LMTD is greater for the high-temperature heater.

References

[1] Gas Turbine World. 2020. GTW Handbook, Pequot Publishing.
[2] Singh DV, Pedersen E. A review of waste heat recovery technologies for maritime applications. Energy Convers Manage 2016;111:315–28. https://doi.org/10.1016/j.enconman.2015.12.073.
[3] Cho SK, Kim M, Baik S, Ahn Y, Lee JI. Investigation of the bottoming cycle for high efficiency combined cycle gas turbine system with supercritical carbon dioxide power cycle. Proceedings of the ASME Turbo Expo 2015. https://doi.org/10.1115/GT2015-43077.
[4] Wright SA, Davidson CS, Scammell WO. Thermo-economic analysis of four sCO2 waste heat recovery power systems. The 5th International sCO2 Power Cycles Symposium 2016. http://sco2symposium.com/papers2016/SystemModeling/059paper.pdf.
[5] Kim MS, Ahn Y, Kim B, Lee JI. Study on the supercritical CO2 power cycles for landfill gas firing gas turbine bottoming cycle. Energy 2016;111:893–909. https://doi.org/10.1016/j.energy.2016.06.014.
[6] Kim YM, Sohn JL, Yoon ES. Supercritical CO2 Rankine cycles for waste heat recovery from gas turbine. Energy 2017;118:893–905. https://doi.org/10.1016/j.energy.2016.10.106.
[7] Yang C, Deng Y, Zhang N, Zhang X, He G, Bao J. Optimal structure design of supercritical CO2 power cycle for gas turbine waste heat recovery: a superstructure method. Appl Therm Eng 2021;198:117515. https://doi.org/10.1016/j.applthermaleng.2021.117515.
[8] Feher EG. The supercritical thermodynamic power cycle. Energy Conversion 1968; 8(2):85–90. https://doi.org/10.1016/0013-7480(68)90105-8.
[9] Angelino G. Carbon dioxide condensation cycles for power production. J Eng Gas Turbines Power 1968;90(3):287–95. https://doi.org/10.1115/1.3609190.
[10] Li MJ, Zhu HH, Guo J, Wang K, Tao Q. The development technology and applications of supercritical CO2 power cycle in nuclear energy, solar energy and other energy industries. Appl Therm Eng 2017;126:255–75. https://doi.org/10.1016/j.applthermaleng.2017.07.173.
[11] Crespi F, Gavagnin G, Sanchez D, Martinez GS. Supercritical carbon dioxide cycles for power generation: A review. Appl Energy 2017;195:152–83. https://doi.org/10.1016/j.apenergy.2017.02.048.
[12] Sanchez Villafana ED, Bueno VMJP. Thermoeconomic and environmental analysis and optimization of the supercritical CO2 cycle integration in a simple cycle power plant. Appl Therm Eng 2019;152(1–12). https://doi.org/10.1016/j.applthermaleng.2019.02.052.
[13] Manente G, Costa M. On the conceptual design of novel supercritical CO2 power cycles for waste heat recovery. Energies 2020;13(2):370. https://doi.org/10.3390/en13020370.
[14] Li B, Wang SS, Wang K, Song L. Comparative investigation on the supercritical carbon dioxide power cycle for waste heat recovery of gas turbine. Energy Convers Manag 2021;228:113670. https://doi.org/10.1016/j.enconman.2020.113670.
[15] Na SI, Kim MS, Baik YJ, Kim M. Optimal allocation of heat exchangers in a Supercritical carbon dioxide power cycle for waste heat recovery. Energy Convers Manage 2019;199:112002. https://doi.org/10.1016/j.enconman.2019.112002.
[16] Alfani D, Binotti M, Macchi E, Silva P, Astolfi M. sCO2 power plants for waste heat recovery: design optimization and part-load operation strategies. Appl Therm Eng 2021;195:117013. https://doi.org/10.1016/j.applthermaleng.2021.117013.
[17] Li B, Wang SS, Xu Y, Song L. Study on the off-design performance of supercritical carbon dioxide power cycle for waste heat recovery of gas turbine. Energy Convers Manag 2021;233:113890. https://doi.org/10.1016/j.enconman.2021.113890.
[18] Song J, Li XS, Ren XD, Gu CW. Performance improvement of a preheating supercritical CO2 (S-CO2) cycle based system for engine waste heat recovery. Energy Convers Manage 2018;161:225–33. https://doi.org/10.1016/j.enconman.2018.02.009.
[19] Khan Y, Mishra RS. Parametric (exergy-energy) analysis of parabolic trough solar collector-driven combined partial heating supercritical CO2 cycle and organic Rankine cycle, Energy Sources, Part A: Recovery. Utilization and Environmental Effects 2020. https://doi.org/10.1080/15567036.2020.1788676.
[20] Wang Z, Jiang Y, Ma Y, Han F, Ji Y, Cai W. A partial heating supercritical CO2 nested transcritical CO2 cascade power cycle for marine engine waste heat recovery: Thermodynamic, economic, and footprint analysis. Energy 2022;261:125269. https://doi.org/10.1016/j.energy.2022.125269.
[21] Bonalumi D, Giuffrida A, Sicali F. Techno-economic investigations of supercritical CO2-based partial heating cycle as bottoming system of a small gas turbine. Energy 2022;252:124066. https://doi.org/10.1016/j.energy.2022.124066.
[22] Bonalumi D, Giuffrida A, Sicali F. A case study of cascade supercritical CO2 power cycle for waste heat recovery from a small gas turbine. Energy Convers Manage X 2022;14:100212. https://doi.org/10.1016/j.ecmx.2022.100212.
[23] Hou S, Wu Y, Zhou Y, Yu L. Performance analysis of the combined supercritical CO2 recompression and regenerative cycle used in waste heat recovery of marine gas turbine. Energy Convers Manage 2017;151:73–85. https://doi.org/10.1016/j.enconman.2017.08.082.
[24] Thanganadar D, Asfand F, Patchigolla K. Thermal performance and economic analysis of supercritical carbon dioxide cycles in combined cycle power plant. Appl Energy 2019;255:113836. https://doi.org/10.1016/j.apenergy.2019.113836.
[25] Liu Y, Zhao Y, Yang Q, Liu G, Li L. Thermodynamic comparison of CO2 power cycles and their compression processes. Case Studies in Thermal Engineering 2020; 21:100712. https://doi.org/10.1016/j.csite.2020.100712.
[26] Pan M, Zhu Y, Bian X, Liang Y, Lu F, Ban Z. Theoretical analysis and comparison on supercritical CO2 based combined cycles for waste heat recovery of engine. Energy Convers Manage 2020;219:113049. https://doi.org/10.1016/j.enconman.2020.113049.
[27] Pan P, Yuan C, Sun Y, Yan X, Lu M, Bucknall R. Thermo-economic analysis and multi-objective optimization of S-CO2 Brayton cycle waste heat recovery system for an ocean-going 9000 TEU container ship. Energy Convers Manage 2020;221:113077. https://doi.org/10.1016/j.enconman.2020.113077.
[28] Carraro G, Danieli P, Lazzaretto A, Boatto T. A common thread in the evolution of the configurations of supercritical CO2 power systems for waste heat recovery. Energy Convers Manage 2021;237:114031. https://doi.org/10.1016/j.enconman.2021.114031.
[29] Monje B, Sanchez D, Savill M, Pilidis P, Sanchez T. A design strategy for supercritical CO2 compressors. Proceedings of ASME Turbo Expo 2014. https://doi.org/10.1115/GT2014-25151.

[30] Monge B, Sanchez D, Savill M, Sanchez T. Exploring the design space of the sCO2 power cycle compressor. The 4th International sCO2 Power Cycles Symposium 2014. http://sco2symposium.com/papers2014/turbomachinery/46-Sanchez.pdf.
[31] Allison TC, Moore J, Pelton R, Wilkes J, Ertas B. Turbomachinery. In: Brun K, Friedman P, Dennis R, editors. Fundamentals and applications of supercritical carbon dioxide (SCO2) based power cycles. Woodhead Publishing, 2017, p. 147-215, https://doi.org/10.1016/B978-0-08-100804-1.00007-4.
[32] Aungier RH. Turbine aerodynamics - Axial-flow and radial-inflow turbine design and analysis. ASME Press 2005.
[33] Aungier RH. Centrifugal compressors - A strategy for aerodynamic design and analysis. ASME Press; 2000.
[34] Manente G, Fortuna FM. Supercritical CO2 power cycles for waste heat recovery: a systematic comparison between traditional and novel layouts with dual expansion. Energy Convers Manage 2019;197:111777. https://doi.org/10.1016/j.enconman.2019.111777.
[35] https://www.nist.gov/srd/refprop, last access on September 30, 2022.
[36] Span R, Wagner W. A new equation of state for carbon dioxide covering the fluid region from the triple-point temperature to 1100 K at pressures up to 800 MPa. J Phys Chem Ref Data 1996;25(6):1509–96. https://doi.org/10.1063/1.555991.
[37] Bergman TL, Lavine AS, Incropera FP, De Witt DP. Fundamentals of Heat and Mass Transfer. John Wiley and Sons; 2011.
[38] Weiland N, Thimsen D. A Practical look at assumptions and constraints for steady state modeling of sCO_2 Brayton power cycles. The 5th International sCO_2 Power Cycles Symposium 2016. http://sco2symposium.com/papers2016/SystemModeling/102paper.pdf.
[39] Musgrove G, Sullivan S, Shiferaw D, Fourspring P, Chordia L. Heat exchangers, In: Brun K, Friedman P, Dennis R, editors. Fundamentals and applications of supercritical carbon dioxide (SCO2) based power cycles, Woodhead Publishing, 2017, pp. 217-244, https://doi.org/10.1016/B978-0-08-100804-1.00008-6.